

Effect of the equilibrium pair separation on cluster structures

Y. Yang and D. Y. Sun

State Key Laboratory of Precision Spectroscopy and Department of Physics,
East China Normal University, Shanghai 200062, China

(Dated: July 16, 2008)

A simple pair potential, which equilibrium pair separation can be varied under a fixed interaction range, has been proposed. The new potential can make both face-centered-cubic(fcc) and body-centered-cubic(bcc) structure stable by simply changing one parameter. To investigate the general effect of the potential shape on cluster structures, the evolution of cluster structures is calculated for different equilibrium pair separations. The small size clusters($N < 25$), which adopt the polytetrahedra, are almost independent on the details of the potential. For the large size clusters($25 < N < 150$), the potential with large equilibrium pair separation trends to stable decahedra and close-packed structure, disordered clusters appear for the potential with small equilibrium pair separation, while for the middle range of equilibrium pair separation, the icosahedra are dominated.

I. INTRODUCTION

Nanoclusters, with the exotic physical and chemical properties, have brought a big chance for future industry in many areas, it also challenges our current theories and models for traditional condensed matters.¹ Until now, many phenomena of nano-system still puzzle physicists, chemists and material scientists. Undoubtedly, any precise description of cluster properties needs the correct structural models. To date few direct measurements of cluster structures are available experimentally,² and much of the current theoretical understanding of cluster structures has been derived from atomic-scale molecular-dynamics(MD) and Monte Carlo(MC) simulations.³

In computer simulations, finding the most stable structure corresponds to search the global minimum of complicated multi-dimensional potential energy surfaces(PES).⁴ The potential energy surfaces of clusters are usually represented by an appropriate energetic model, such as that based on *ab-initio* method, tight-binding(TB) models, or (Semi)empirical interaction potentials. The model clusters, described by Lennard-Jones(LJ) and Morse potentials, have been studied extensively(e.g., Refs.³ and references therein). Metal clusters are also widely studied using both DFT and classical many-body potentials(e.g., Refs.^{3,5,6} and references therein). The studies were even extended to large molecule systems^{7,8,9,10,11,12,13,14,15,16,17} and multi-matter system.^{18,19,20,21,22,23,24,25,26} Many exotic structures, which is probably forbidden in bulk materials, have been reported in the previous studies. The excellent example includes, the cage structures of carbon,²⁷ the Icosahedra(IH)^{28,29} and decahedra(DH)^{30,31} based atomic shell structures of metal clusters, and the recent found cage structures of gold clusters,^{32,33} etc.

Indubitably the cluster structures are determined by the details of the interatomic interaction. One of the current focuss is to examine the general structural effects of the different contributions to the interaction. Doye and Wales found that the Friedel type oscillation in atomic potentials can strongly modulate the cluster

structures.^{34,35,36} The original and mechanism of disordered structure in metal clusters were studied in term of the different many-body forms.^{37,38} Baletto *et al* have shown how the potential forms affect the crossover size between different structural motifs (icosahedra, decahedra, and truncated octahedra).³⁹ Michaelian *et al* have made a comparison of the global minimum structure for different many-body potentials.⁴⁰ Doye and Wales investigated the structural consequence issue for a set of Sutton-Chen families of potentials.⁴¹ Gong and his coworkers have studied the relativistic effect on the structure of gold clusters, which leads the presences of cage-like structures.^{32,33}

For studying the general effects of potential shapes on cluster structures, Doye and Wales suggested to consider a potential which is simple enough that one can comprehend the effects of any changes to its form. This method has been used to investigate the effect of the potential range and anisotropy on the cluster structures. Braier *et al* first made the study on six- and seven-atom clusters bound by the Morse potential for different interaction range.⁴² A similar study was preformed on other model potentials. Rey and Gallego have shown how the structures and melting behavior of hard-core Yukawa clusters changing with the range of attractive Yukawa tail.⁴³ Based on the generalized LJ, Morse, and Born-Mayer potentials, Amano *et al* recently investigated the structure change with the potential shape.⁴⁴ Doye and Wales made a systematic search of the PES of Morse clusters as a function of the interaction range. They found that, decreasing the range results in destabilizing strained structures.^{45,46,47,48} The general trend have been used to explain the growth sequences of other systems.⁷

Despite substantial efforts by many researchers, our knowledge about the relationship between cluster structure and potential shape is still limited on a few factors, specially the effect of the interaction range. Although the interaction range does play an important role for an interatomic potential, other factors also should not be neglected. Obviously the further studies along this line are needed. Another important factors could be the

equilibrium pair separation(d_{EPS}), which reflect the size of atoms. Specially, for a fixed interaction range, how the equilibrium pair separation(d_{EPS}) affect the cluster structure is worthy to be answered. Physically, changing of d_{EPS} corresponds to changing the atomic size. The importance of the atomic size issue has been shown in recent studies on C_{60} .⁴⁹ In present paper, by introducing a simple model potential, which has the fixed interaction range but variable equilibrium pair separation, or equally speaking 'the atomic size', we have studied the effect of d_{EPS} on the cluster structures.

The remainder of the paper is organized as follows. The following section describes the new developed model potential and computational details. The cluster structures for a few selected parameters are presented in Sec. III. The conclusions drawn from this work are summarized in Sec. IV.

II. COMPUTATIONAL DETAILS

The potential we used was originally obtained from the effective pair potential⁵⁰ of EAM potential for iron,^{51,52} then we re-parameterize it in the current form:

$$\Phi(r_{ij}) = \begin{cases} \varepsilon[\frac{r_{ij}}{\sigma} - 2.5]^3[\gamma - 1.44719(\frac{\sigma}{r_{ij}})]; r_{ij} \leq 2.5\sigma \\ 0; r_{ij} > 2.5\sigma \end{cases} \quad (1)$$

where ε and σ is energy and length unit respectively. r_{ij} denotes the distance between atom i and j . γ is an adjustable parameter, which determines the d_{EPS} of the potential. The higher value of γ gives a shorter d_{EPS} . ε is chosen to keep the potential well depth equal to one for each γ , and σ equals to one for all case studied. Figure 1 shows the new potential with a few selected γ of 0.8, 0.9, 0.95, 1.0, 1.05, 1.1, 1.2. For comparing, this figure also shows the Morse and LJ potential, where they have been fitted to have the same curvature at the bottom of the potential well as the present one. From this figure, one can see that, changing γ corresponds to the alternation of the equilibrium pair separation, also can be regarded as changing the atomic size. Of course, by changing γ , the stiffness of the potential is also changed, which is similar to the Morse potential in this point. Comparing to Morse and LJ potential, the new one is softer in repulsive part and stiffer in attractive part, and shorter in interaction range.

Another feature of the current potential is that it can make both fcc and bcc stable by varying γ . Table 1 presents the cohesive energy of fcc and bcc phase as a function of γ . The both fcc and bcc have the same energy at zero temperature at $\gamma=1$. For γ larger than one, bcc phase is stable over fcc, while the smaller γ favors fcc phase. The reason is that, for large γ , the potential well becomes more and more flat. In this case, the dominated interaction in bcc is the both first and second nearest neighbors totally 14 atoms, while only 12 first

nearest neighbors are contributed to energy in fcc due to the limited interaction range. It needs to point that the Morse potential always make the fcc more stable over bcc. This is the major difference between the present potential and Morse one. This potential is also similar to the Johnson potential for bcc Iron,⁵³ which implies that this form may represent some major physics of bcc based metals.

To optimize the cluster structure, we first search the global minimum among all the known structures for each potential and cluster size⁵⁴ using the steepest-descent method. Then we make further exploration for most stable structure with the generalized-simulated-annealing algorithm, which has been shown in previous work as a powerful and efficient procedure.⁵⁵ The most stable structure then can be found among these structures.

III. RESULTS AND DISCUSSIONS

Fig.2 plots the second difference of energy($\Delta_2 E = E(N+1) + E(N-1) - 2E(N)$) as a function of cluster sizes for all studied γ . From top to bottom, it corresponds to the γ from 0.8 to 1.2 respectively. For size smaller than 24, all the curves have the same trend. This implies that the structures are less dependent on the details of potentials at small sizes, which is similar to the case in Morse potentials.⁴⁸ For all γ except 0.8, around size from 135 to 147, $\Delta_2 E$ is almost equal to zero. This is because these clusters are based on IH_{147} cluster by taking a few atoms among its 12 vertex atoms. These vertex atoms are all equal due to the symmetry. As the size larger than 24, the differences of these curves begin to emerge. The curve of $\gamma=0.8$ is evidently different from others for size larger than 23. $\gamma=0.9$ and 0.95 are similar each other in whole range of sizes. The major trends of $\gamma=1.0, 1.05, 1.1$ and 1.2 are close in the most ranges. These differences are the reflection of different structure type as discussing below.

Peaks in $\Delta_2 E$ correspond to clusters which are stable compared to adjacent sizes and have been found to correlated with magic numbers in mass spectra of clusters. We note that there are two types of peaks in $\Delta_2 E$. One type of peaks corresponds to especially stable clusters, such as $N=13, 55, 147$, the closed-shell IH structures. Another one is directly related to the change of structural types. For example, $\Delta_2 E$ for $\gamma=0.8$ has several this type of peaks for $N>100$, which actually correspond to the close-packed (CP) clusters changing to the DH motifs.

A few of structural types, i.e., polytetrahedra(PT), polytetrahedral involve an ordered array of disclinations($PT-d$) IH , DH , CP and disordered(DIS) structures, were found in present study. About these structures, the detailed description can be found elsewhere, (e.g., Refs.³ and references therein) we briefly summary here. PT is made by packing five smallest tetrahedra sharing a common edge. The PT can further reduce its strain by involve an ordered array of

disclinations(hereafter labeled as *PT-d*), where there are more than five smallest tetrahedra sharing a common edge. Both *PT* and *PT-d* can be naturally divided up into tetrahedra with atoms at their corners. *IH* can be decomposed into 20 fcc tetrahedra sharing a common vertex in the central site. A close-shell *IH* has 20 triangular fcc(111) faces and 12 vertices. A decahedron is made up of two pentagonal pyramids sharing a common basis. It has a single fivefold axis and is formed by five tetrahedra sharing a common edge along the fivefold axis. Both *IH* and *DH* can have close geometry shell structure. *CP* is a pieces of fcc structure. The truncated octahedron is one of *CP*. By contrast, close-packed structures are composed of octahedra and tetrahedra. *DIS* is that the clusters can hard be identified with any order structure.

Most *PT* clusters are observed at small sizes. Specially all clusters less than 24 atoms are *PT* type, and most of them are identical for all γ at the same size. This means that the cluster structures are less relevant with the details of potential. Fig.3 shows the small size *PT* clusters of $N=4-23$. These clusters are on a *PT* growth sequence. For example, the 7-atom cluster has a structure in the shape of a pentagonal bipyramid, which can be viewed as packing of five small tetrahedra by introducing some inherent strains. The clusters larger than seven atoms grow by introducing more new tetrahedra on its surface. The *PT* growth sequence keeps and leads to the 13-atom cluster, which is commonly regarded as an icosahedron, however, it is also a *PT* according to Hoare's description, and can be view as the packing of 20 small tetrahedra.^{56,57} The 19-atom cluster is packed by small tetrahedra on the surface of the 13-atom cluster. The clusters grow further by packing around the waist of the 19-atom cluster to larger clusters. The *PT* growth sequence is maintained and strain is also accumulated. There are a few clusters in the size range smaller than 24, which did not follow the growth sequence described above, but still has *PT* structure. The exceptions are also listed in the Fig.3, which is $N=8,21,23$ for $\gamma=1.2,1.1$, and 0.8 respectively. For cluster with $N=8$ and $\gamma=1.2$, which is not the normal *PT* structure, is the fraction of a bcc structure. $N=8$ cluster can also be viewed as a positive-disclination *PT* cluster(only four tetrahedra sharing a common edge), it has more positive strain than normal *PT*.

Fig.4 presents the extension of the *PT* growth sequence based on the small size clusters. 34-atom cluster is complete form of the waist-packing pattern based on the 19-atom cluster. The larger *PT* clusters($35 < N < 55$) are based on the 34-atom cluster, which is similar to the growth mode form 13-atom *PT* to 19-atom.

With increasing of cluster size, the positive strain is also accumulated rapidly in *PT*. To reduce the positive strain, *PT-d* was observed. Fig.5 presents a few selected *PT-d* clusters. This type of clusters has been discussed in several papers.^{35,47,56} *PT-d* structure is different from *PT* by introducing six tetrahedra share a common edge in some sites. Although disclinations is unfavor in local,

it does result in the decrease of global strain of clusters. In fact, this structure is similar to the square-triangle Frank-Kasper phases usually used in the quasi-crystals.^{58,59,60,61}

The *IH* clusters appear following the *PT-d* clusters at larger sizes. Some selected *IH* clusters are listed in the Fig.6. Each cluster is given in the side view and the top view. There are many discussions in previous papers about *IH*.³ The *IH* clusters can be viewed as packing atoms based on a 13-atom pentadecahedron but not a 13-atom Icosahedron. Usually, comparing with *PT*, *IH* clusters have larger fcc(111) surface and shell-like structure. These *IH* clusters are stable due to their extreme large fcc(111) surface and less strains comparing to *PT*. For any *IH* based cluster, it can always form a closed-shell icosahedron by packing enough atoms on it. There are also a few *IH* clusters(see Fig.7), which are interesting because they are not the fracture of next closed-shell icosahedron, but the fracture of the larger icosahedron. For example, *IH* clusters of $N=48,50$ are not the fracture of $N=55$ icosahedron, but the fracture of $N=147$ icosahedron. Also clusters with $N=89,90(\gamma = 0.8)$ and $N=62,65(\gamma = 0.9 - 1.0)$ are the fracture of $N=561$ icosahedron. These clusters were discussed by Baletto *et al*⁶² as natural pathway to the growth of larger *IH* clusters.

Fig.8 shows some *DH*, *CP* and *DIS* structures. Both *DH* and *CP* clusters are found for the small value of γ . For simple pair potentials, the smaller *DH* and *CP* can only exist for very narrow potential, or potential with very large d_{EPS} , such as C_{60} clusters. *CP* definitely have the same structure with fcc crystal, and *DH* is also more close to fcc structure over *PT* and *IH*. Disorder clusters appear for larger γ around 1.2, where the potential is much flat around the bottom. Some disordered clusters are in fact a serious distorted ordered structures. For example, distorted *IH*($N=85,103,\gamma=1.2$) are listed. There are many disordered structures are hard to be recognized based on any ordered structures($N=38,\gamma=1.2$). There are also some interpenetrated clusters, which exhibit the combination of two type structures.⁴⁷ The interpenetrated clusters were found during the structure motif changing. The remarkable feature of these clusters is that it exhibits different structural character by looking from different direction, for examples, the cluster of $N=59$ and $\gamma = 1.2$ is found between *PT* and *IH*.

Fig.9 plots the zero temperature structure 'phase diagram' as a function of both cluster size and γ . It can be seen that, the smaller γ , the more *DH* and *CP* clusters, and the less disorder clusters. For $\gamma=0.8$, the structure is dominated by the *DH* and *CP*. And only one *DH* and one *CP* clusters are found in the potentials of $\gamma > 0.9$. The number of *PT* clusters increase with increasing of γ . For different potentials, this growth sequence stops at the different sizes($N=24(\gamma=0.8), N=31(\gamma=0.9), N=34(\gamma=0.95), N=37(\gamma=1.0,1.05,1.1), N=43(\gamma=1.2)$). *PT-d* clusters favor the size within 25 to 107. After the *PT-d* motif first emerges at $\gamma=0.95$, its number increases with the increasing of γ , and reaches the maximum

around $\gamma=1.05$. As γ continues to increase, the distribution of *PT-d* motif begins to reduce. At $\gamma=1.2$, only seven *PT-d* clusters are found. The disordered clusters first emerge at the large size between the two magic number $N=55$ and $N=147$ at $\gamma=1.0$, and its distribution increase as the increasing of γ . At the value of $\gamma=1.2$, it is dominated by the disordered cluster. The *IH*-based clusters usually appear in larger sizes. *IH* clusters dominate for value of $\gamma=0.9$ and 0.95 , and its number decreases for both γ larger than 0.95 and smaller 0.9 .

Since clusters have non-neglectful surface effect and large deformation in contract with its bulk crystal, the competition between the deformation(strain) and surface energy plays the key role in determining cluster structures. According to this consideration, we can give a qualitative explanation for the existing of each structural type. Small size clusters have very large surface-volume ratio, thus the surface effect is dominated. *PT* clusters are abundant at small sizes due to its the lowest energy surface, fcc(111) surface. The dominant geometric effect can not be easily affected unless for enough strong atomic interaction. For Morse potential,⁴⁸ only an extreme narrow potential can breaks the *PT* motif. Since strains in *PT* clusters increase rapidly due to continuously packing tetrahedra, *PT-d* replace the *PT* with size increasing due to the partially release of strains. Further increasing sizes, both *PT* and *PT-d* are more and more unfavorable, thus the *IH* clusters appear. *IH* clusters have the similar surface as *PT* and *PT-d*, but the inner strain is much reduced when taking *IH* arrangement. This is the reason why the *IH* clusters appear after *PT-d* ones.

Among *IH*, *DH* and *CP* structure, *IH* has the lowest surface energy and largest deformation energy, *CP* is opposite, while *DH* is in the middle. For small γ (narrow potential), the structure with large deformation(strain) is unfavorable, *CP* and *DH* are dominated. The deformation(strain) can be neglected for largest γ (more flat potential), the *PT* and disordered clusters are favorable. For middle value of γ , the *PT-d* and *IH* are appeared. Generally *DIS* should have the largest strain energy, thus it can only survive for flat potential, this is the case of large γ in present case. The cluster distribution is in agreement with the Doye's qualitative principle that decreasing the range of the pair-potential(the width of po-

tential well) has the effect of destabilizing strained structures. It needs to point that a quantitative analysis is necessary for detailed understanding.

The most stable structure of bulk phase is bcc for $\gamma > 1$, however only one cluster has the character as a fraction of bcc, which is the one with $N=8$ and $\gamma=1.2$. On the contrary, a large number of *IH* and *PT* clusters are found for $\gamma > 1$. The main reasons come from the surface effect of small cluster, which result in the clusters adopting the most close packed fcc(111) surface. However, there could be the inherent competition between fcc and bcc, the existence of *DIS* and *PT-d* clusters could be the results for $\gamma > 1$.

IV. SUMMARY

In this paper, we have studied how the change of equilibrium pair separation (or atomic size) for a fixed interaction range affects the favored structures of atomic clusters. To do so, a simple pair potential, which equilibrium pair separation can be varied under a fixed interaction range by changing one of the potential parameters has been proposed. This potential also can make both face-centered-cubic structure and body-centered-cubic stable by changing the parameter. The evolution of cluster structures are calculated for several sets of parameters. Our results show that, the potential with large equilibrium pair separation(larger atomic size) favors *DH* and *CP* structures, disordered clusters appear for the potential with small equilibrium pair separation, while for the middle range of equilibrium pair separation, the *IH* structures are dominated. Present observation conforms the Doye and Wales's qualitative principle that decreasing the range of the pair-potential has the effect of destabilizing strained structures.

Acknowledgments

This research was supported by the National Science Foundation of China, Shanghai Project for the Basic Research. The computation is performed in the Supercomputer Center of Shanghai.

¹ H. S. Nalwa, *Encyclopedia of Nanoscience and Nanotechnology* (American Scientific, New York, 2004).

² L. D. Marks, Rep. Prog. Phys. **57**, 603 (1994).

³ F. Baletto and R. Ferrando, Rev. Mod. Phys. **77**, 371 (2005).

⁴ D. J. Wales, *Energy Landscapes with Applications to Clusters, Biomolecules and Glasses* (Cambridge University, Cambridge, England, 2003).

⁵ R. C. Longo, E. G. Noya and L. J. Gallego, J. Chem. Phys. **122**, 226102 (2005).

⁶ R. C. Longo, E. G. Noya and L. J. Gallego, Phys. Rev. B

72, 174409 (2005).

⁷ J. P. K. Doye and D. J. Wales, Chem. Phys. Lett. **247**, 339 (1995).

⁸ J. P. K. Doye and D. J. Wales, Chem. Phys. Lett. **262**, 167 (1996).

⁹ J. P. K. Doye, D. J. Wales, W. Branz and F. Calvo, Phys. Rev. B **64**, 235409 (2001).

¹⁰ J. Hernández-Rojas, J. Bretón, J. M. Gomez Llorente and D. J. Wales, J. Chem. Phys. **121**, 12315 (2004).

¹¹ J. Hernández-Rojas, J. Bretón, J. M. Gomez Llorente and D. J. Wales, J. Phys. Chem. B, **110**, 13357 (2006).

- ¹² M. P. Hodges and D. J. Wales, Chem. Phys. Lett. **324**, 279 (2000).
- ¹³ S. Maheshwary, N. Patel, N. Sathyamurthy, A. D. Kulkarni and S. R. Gadre, J. Phys. Chem.-A **105**, 10525 (2001).
- ¹⁴ D. J. Wales and M. P. Hodges, Chem. Phys. Lett. **286**, 65 (1998).
- ¹⁵ H. M. Lee, S. B. Suh, and K. S. Kim, J. Chem. Phys. **115**, 7331 (2001).
- ¹⁶ T. James, D. J. Wales and J. Hernández-Rojas, Chem. Phys. Lett. **415**, 302 (2005).
- ¹⁷ B. S. González, J. Hernández-Rojas, D. J. Wales, Chem. Phys. Lett. **412**, 23 (2005).
- ¹⁸ J. Jellinek and E. B. Krissinel, Chem. Phys. Lett. **258**, 283 (1996).
- ¹⁹ G. Rossi, A. Rapallo, C. Mottet, A. Fortunelli, F. Baletto and R. Ferrando, Phys. Rev. Lett. **93**, 105503 (2004).
- ²⁰ D. Sabo, J. D. Doll and D. L. Freeman, J. Chem. Phys. **121**, 847 (2004).
- ²¹ A. Rapallo et al., J. Chem. Phys. **122**, 194308 (2005).
- ²² J. P. K. Doye and L. Meyer, Phys. Rev. Lett. **95**, 063401 (2005).
- ²³ R. Ferrando, A. Fortunelli and G. Rossi, Phys. Rev. B **72**, 085449 (2005).
- ²⁴ R. C. Longo, E. G. Noya and L. J. Gallego, J. Chem. Phys. **122**, 083311 (2005).
- ²⁵ R. C. Longo, E. G. Noya, A. Vega and L. J. Gallego, Solid State Commun. **140**, 480 (2006).
- ²⁶ B. C. Curley, G. Rossi, R. Ferrando and R. L. Johnston, Eur. Phys. J. D **43**, 53 (2007).
- ²⁷ H. Kroto, J. Heath, S. O'Brien, R. Curl and R. Smalley, Nature **318**, 162 (1985).
- ²⁸ A. L. Mackay, Acta Crystallogr. **15**, 916 (1962).
- ²⁹ T. P. Martin, Phys. Rep. **273**, 199 (1996).
- ³⁰ S. Ino, J. Phys. Soc. Jpn. **27**, 941 (1969).
- ³¹ L. D. Marks, Philos. Mag. A **49**, 81 (1984).
- ³² X. Gu, M. Ji, S. H. Wei, X. G. Gong, Phys. Rev. B **70**, 205401 (2004).
- ³³ M. Ji, X. Gu, X. Li, X. G. Gong, J. Li, L. S. Wang, Angew. Chem. Int. Edit. **44**, 7119 (2005).
- ³⁴ J. P. K. Doye, D. J. Wales and S. I. Simdyankin, Faraday Discuss. **118**, 159 (2001).
- ³⁵ J. P. K. Doye and D. J. Wales, Phys. Rev. Lett. **86**, 5719 (2001).
- ³⁶ J. P. K. Doye, D. J. Wales, F. H. M. Zetterling and M. Dzugutov, J. Chem. Phys. **118**, 2792 (2003).
- ³⁷ J. M. Soler, M. R. Beltrán, K. Michaelian, I. L. Garzón, P. Ordejón, D. Sánchez-Portal and E. Artacho, 2000, Phys. Rev. B **61**, 5771 (2000).
- ³⁸ J. P. K. Doye, Phys. Rev. B **68**, 195418 (2003).
- ³⁹ F. Baletto, R. Ferrando, A. Fortunelli, F. Montalenti and C. Mottet, J. Chem. Phys. **116**, 3856 (2002).
- ⁴⁰ K. Michaelian, N. Rendón and I. L. Garzón, Phys. Rev. B **60**, 2000 (1999).
- ⁴¹ J. P. K. Doye and D. J. Wales, New J. Chem. **22**, 733 (1998).
- ⁴² P. A. Braier, R. S. Berry and D. J. Wales, J. Chem. Phys. **93**, 8745 (1990).
- ⁴³ C. Rey and L. J. Gallego, Phys. Rev. E **53**, 2480 (1996).
- ⁴⁴ C. Amano, M. Komuro, S. Mochizuki, H. Urushibara and H. Yamabuki, J. Mole. Struct.:THEOCHEM **758**, 41 (2006).
- ⁴⁵ J. P. K. Doye and D. J. Wales, J. Phys. B **29**, 4859 (1996).
- ⁴⁶ J. P. K. Doye and D. J. Wales, Science **271**, 484 (1996).
- ⁴⁷ J. P. K. Doye and D. J. Wales, J. Chem. Soc. Faraday Trans. **93**, 4233 (1997).
- ⁴⁸ J. P. K. Doye, D. J. Wales and R. S. Berry, J. Chem. Phys. **103**, 4234 (1995).
- ⁴⁹ M. H. J. Hagen, E. J. Meijer, G. C. A. M. Mooij, D. Frenkel and H. N. W. Lekkerkerker, Nature **365**, 425 (1993).
- ⁵⁰ A. E. Carlsson, Solid State Phys. **43**, 1 (1990).
- ⁵¹ G. J. Ackland, D. J. Bacon, A. F. Calder and T. Harry, Philos. Mag. A **75**, 713 (1997).
- ⁵² M. I. Mendelev, S. Han, D. J. Srolovitz, G. J. Ackland, D. Y. Sun and M. Asta, Philos. Mag. **83**, 3977 (2003).
- ⁵³ R. A. Johnson and D. J. Oh, J. Mater. Res. **4**, 1195 (1989).
- ⁵⁴ The Cambridge Cluster Database, D. J. Wales, J. P. K. Doye, A. Dullweber, M. P. Hodges, F. Y. Naumkin F. Calvo, J. Hernández-Rojas and T. F. Middleton, URL <http://www-wales.ch.cam.ac.uk/CCD.html>.
- ⁵⁵ Y. Xiang, D.Y. Sun, W. Fan and X.G. Gong, Phys. Lett. A **233**, 216 (1997).
- ⁵⁶ J. P. K. Doye, J. Chem. Phys. **119**, 1136 (2003).
- ⁵⁷ M. R. Hoare and P. Pal, Adv. Phys. **20**, 161 (1971).
- ⁵⁸ F. C. Frank and J. S. Kasper, Acta Crystallogr. **11**, 184 (1958).
- ⁵⁹ F. C. Frank and J. S. Kasper, Acta Crystallogr. **12**, 483 (1959).
- ⁶⁰ D. P. Shoemaker and C. B. Shoemaker, *Introduction to Quasicrystals*, edited by M. V. Jaric (Academic, London, 1988), pp. 1-57.
- ⁶¹ D. Shechtman, I. Blech, D. Gratias and J. W. Cahn, Phys. Rev. Lett. **53**, 1951 (1984).
- ⁶² F. Baletto, C. Mottet and R. Ferrando, Phys. Rev. B **63**, 155408 (2001).
- ⁶³ R. H. Leary, and J. P. K. Doye, Phys. Rev. E **60**, R6320 (1999).

TABLE I: The cohesive energy of both fcc and bcc for different sets of γ and ε , where E_{bcc} and E_{fcc} are the cohesive energy for bcc and fcc structures respectively, and a_{bcc} and b_{fcc} are the lattice constants for bcc and fcc structures respectively. For $\gamma < 1.0$, fcc phase is more stable, while $\gamma > 1.0$ bcc structure is more stable. At $\gamma = 1.0$, fcc and bcc have the same cohesive energy.

γ	ε	E_{bcc}	E_{fcc}	a_{bcc}	a_{fcc}
0.80	98.496	-5.326	-6.000	2.222	2.778
0.90	29.415	-5.762	-6.000	2.036	2.557
0.95	18.760	-5.848	-6.001	1.932	2.457
1.00	12.786	-6.036	-6.036	1.859	2.361
1.05	9.168	-6.178	-6.124	1.793	2.264
1.10	6.844	-6.292	-6.252	1.730	2.176
1.20	4.172	-6.604	-6.547	1.589	2.021

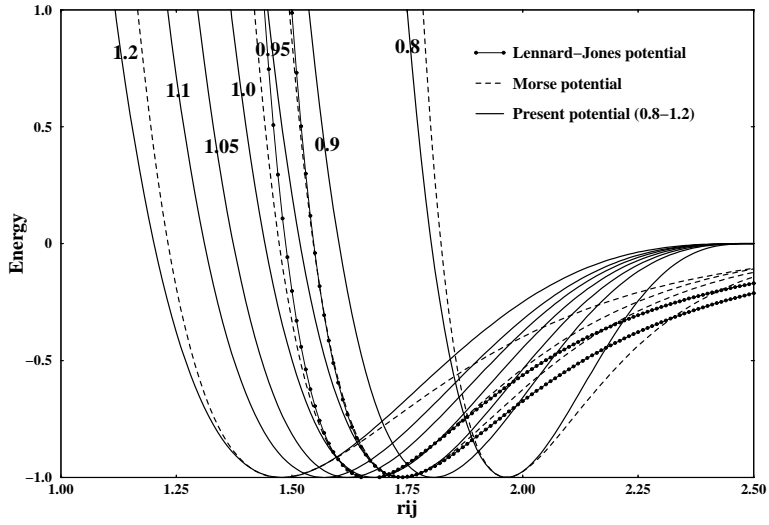


FIG. 1: The new potential(solid line) with a few selected γ of 0.8,0.9,0.95,1.0,1.05,1.1,1.2. For comparing, Morse(dashed line) and LJ(dotted-solid line) potential are also shown, which has been fitted to have the same curvature at the bottom of the potential well as the present one.

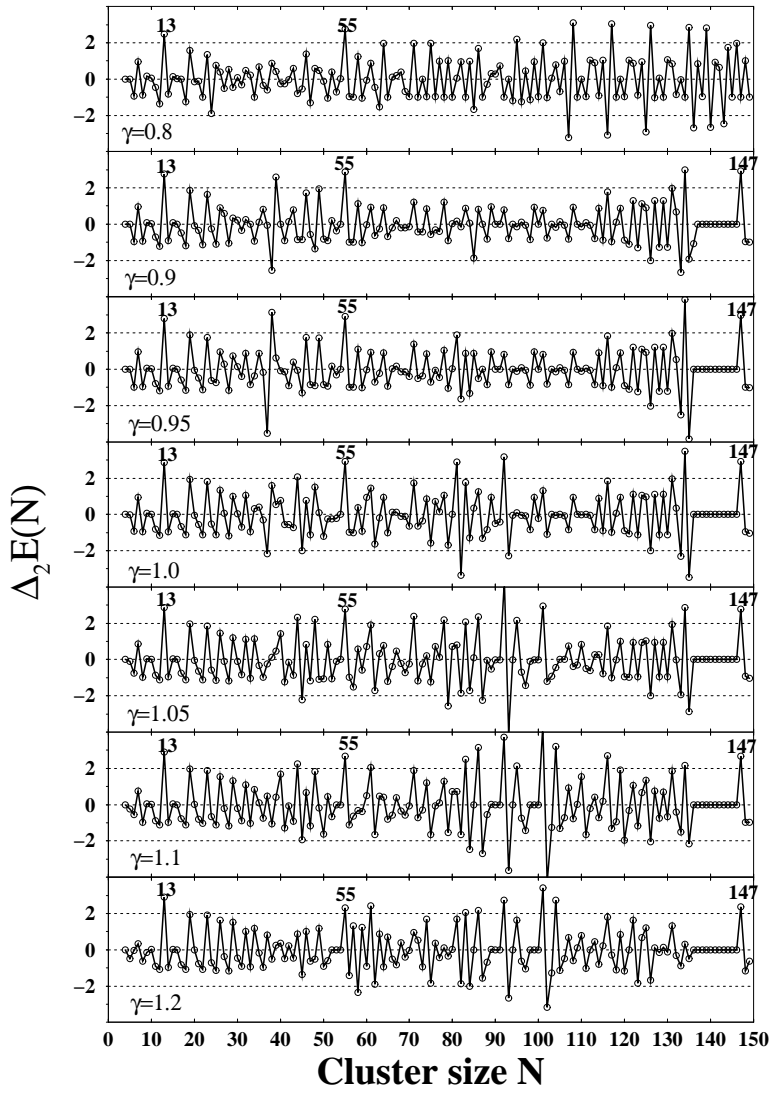


FIG. 2: The second energy difference ($\Delta_2 E$) as a function of cluster size for all γ . Peaks in $\Delta_2 E$ correspond to clusters which are stable compared to adjacent sizes.

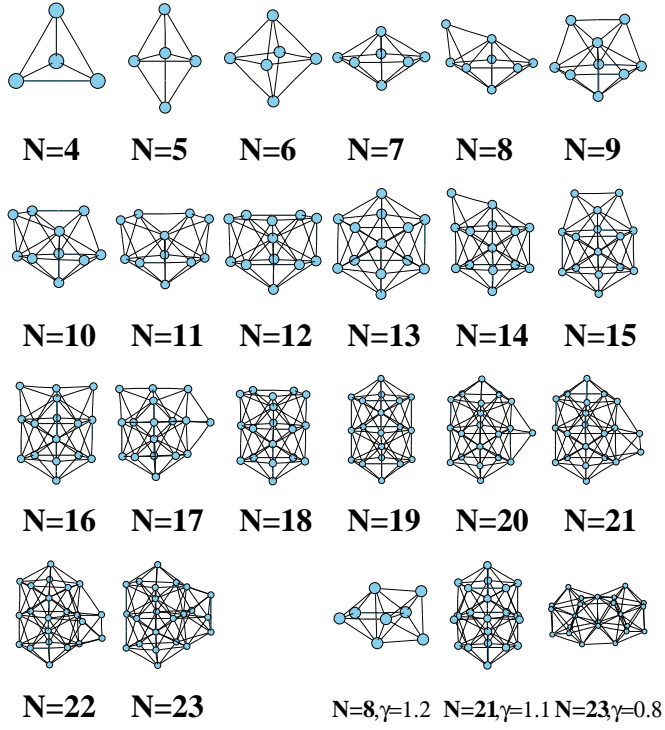


FIG. 3: The small size polytetrahedral clusters of $N=4-23$. Most of them are identical for all γ at the same size. The exceptions are $N=8, 21, 23$ for $\gamma=1.2, 1.1$, and 0.8 respectively.

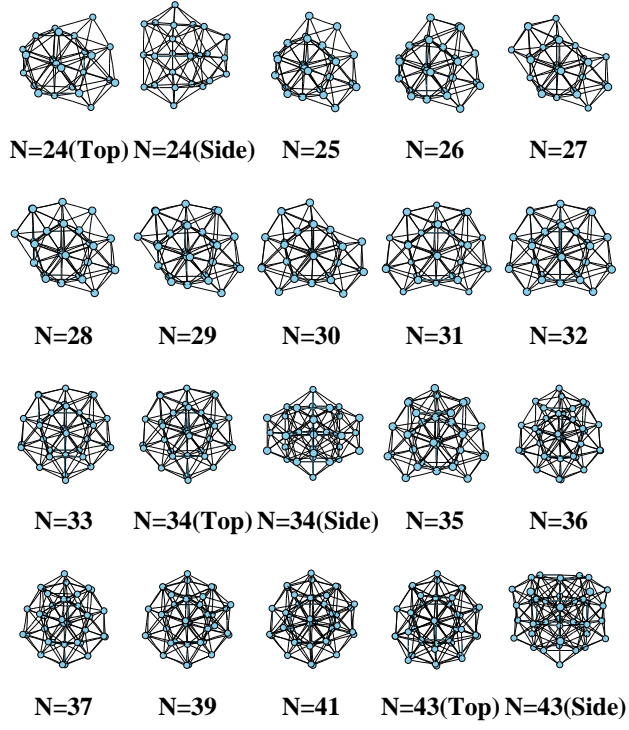


FIG. 4: The extension of the polytetrahedral growth sequence based on the small size clusters.

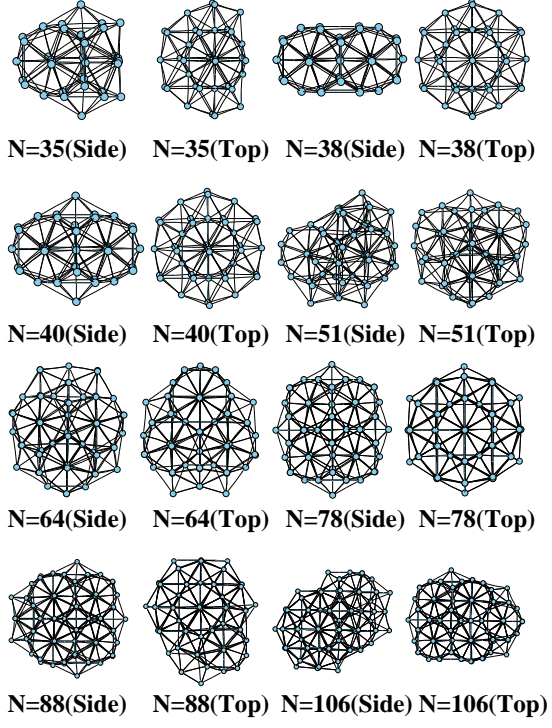


FIG. 5: A few selected PT - d clusters.

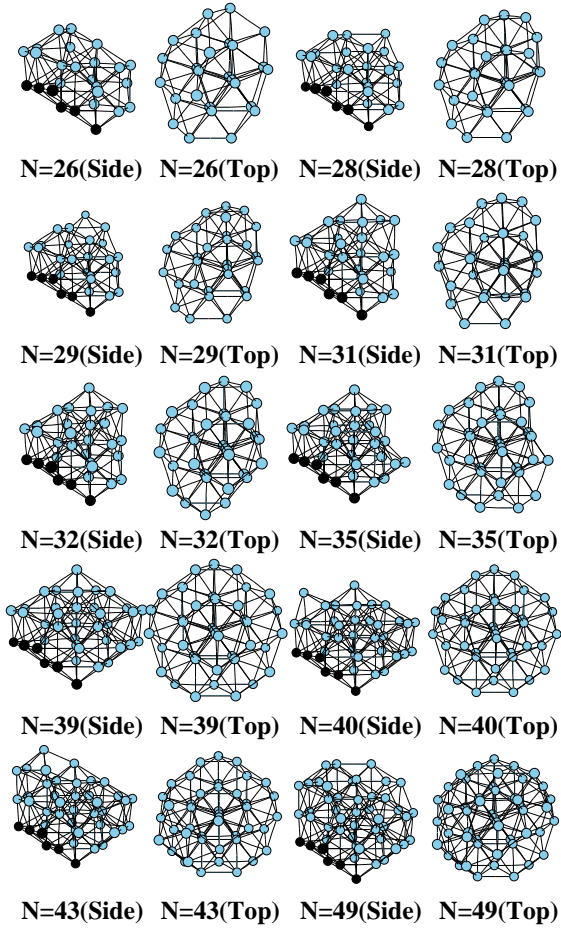


FIG. 6: Some selected IH clusters. Each cluster presented in the side view and the top view, with a 6-atom fcc(111) facet marked in the side view.

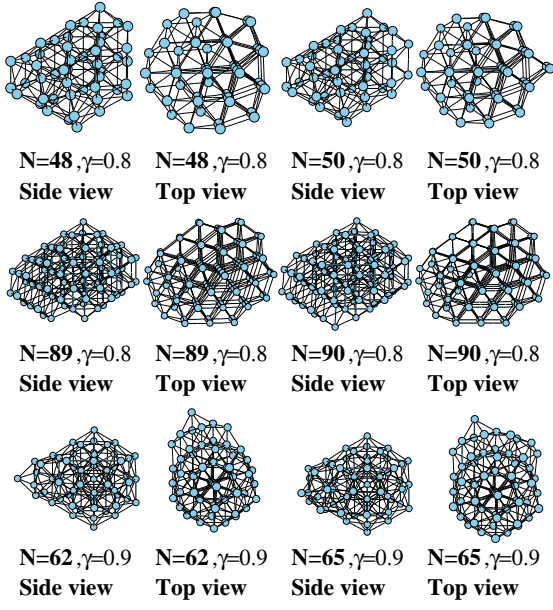


FIG. 7: Some IH clusters are a fraction of larger closed-shell icosahedrons. The clusters with $N=48$ and 50 are the fracture of $N=147$ icosahedron; and $N=89, 90$ ($\gamma = 0.8$) and $N=62, 65$ ($\gamma = 0.9 - 1.0$) are the fracture of $N=561$ icosahedron.

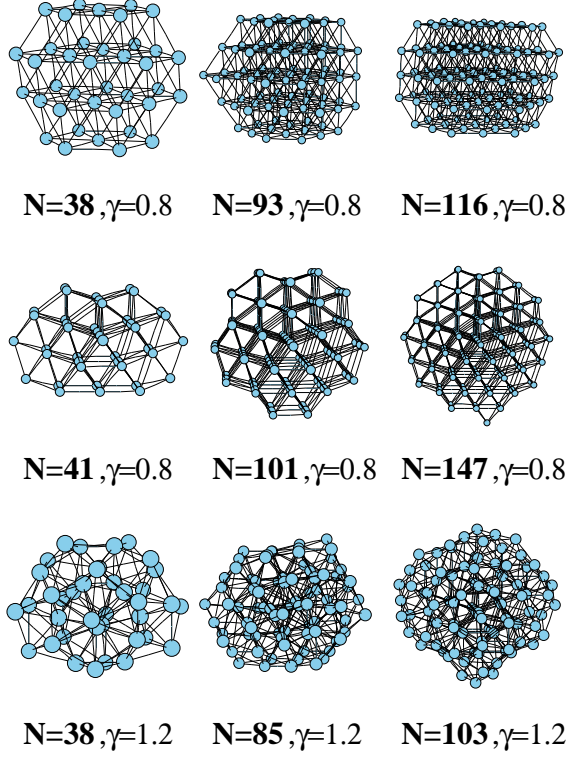


FIG. 8: Some *DH*, *CP* and *DIS* clusters, Top row: *CP* clusters; Middle row: *DH* clusters; Bottom row: *DIS* clusters.

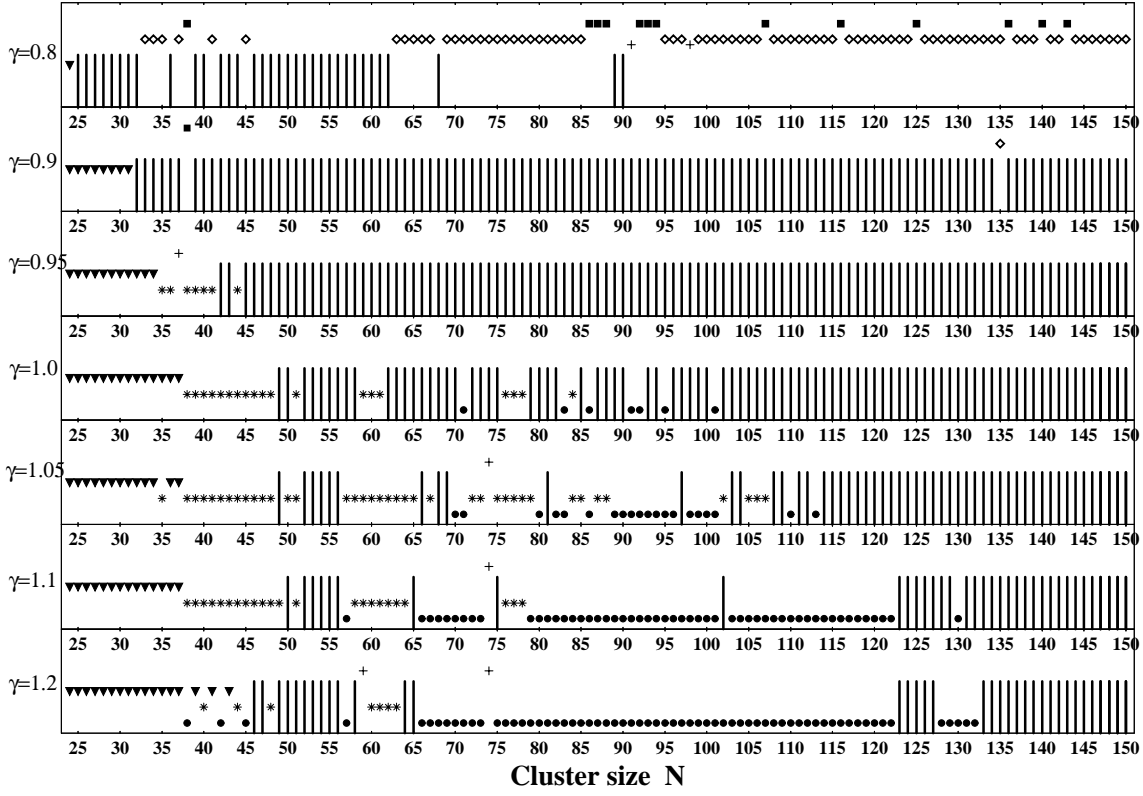


FIG. 9: The zero temperature structural 'phase diagram' as a function of both size and γ . From left, 'Filled triangles' for PT , 'Stars' for $PT-d$ and 'Vertical lines' for IH . 'Filled square' for CP , 'Open diamond' DH , 'Plus' for some minor structure including interpenetrated clusters, a truncate tetrahedra($N=91$, $\gamma=0.8$),⁹ and a rare tetrahedron($N=98$, $\gamma=0.8$).⁶³